

A Physics Based Model for the RTD Quantum Capacitance

Roger Lake and Junjie Yang

Manuscript received May 22, 2002. This work was supported in part by the NSF.

R. Lake and J. Yang are with the Department of Electrical Engineering, University of California, Riverside, CA 92521-0204 USA. (corresponding author R. Lake; phone 909-787-2122; fax: 909-787-2425; e-mail: rlake@ieee.org).

Abstract

A simple derivation of the form for the compact model of the quantum capacitance in a resonant tunneling diode (RTD) is presented. The quantum capacitance is shown to reduce the resistive cutoff frequency. The implementation of the model into SPICE is described. The distorting effect of the strongly non-linear quantum capacitance on an oscillator circuit is demonstrated in a SPICE simulation. The non-linearity becomes important for the highest frequency applications when the RTD capacitance is comparable to the capacitance in the rest of the circuit.

Keywords

Semiconductor device modeling, Resonant tunnel diodes, Circuit modeling, Capacitance, Tunnel diode oscillators

I. INTRODUCTION

The physics based SPICE model introduced in [1] and enhanced in [2] has been used in high-speed digital, mixed signal, and analog circuit design of hybrid resonant tunnel diode (RTD) / HEMT or RTD/HBT circuits. One interesting feature that is absent from the model is the quantum capacitance [3], [4], [5], [6], [7], [8], [9]. Because of the quantum capacitance, the capacitance of an RTD peaks in the center of the negative differential resistance region which is precisely where one wishes to bias the device for linear applications. Using quantum simulations as a guide, we derive an analytic expression for the quantum capacitance, add it to the SPICE model described in [1-2], analyze its effect on the resistive cutoff frequency, and demonstrate a SPICE simulation of an oscillator circuit.

Our approach is to use physical device simulation, NEMO [10], to gain physical insight and to provide qualitatively correct I-V and C-V responses for verification of the compact model for SPICE. Our test device is an InAs / AlSb RTD optimized for high frequency response based on the original device of [11]. The device geometry consists of a 1.5 nm (5 monolayer) emitter barrier, a 7.9 nm well, and a 0.9 nm (3 monolayer) collector barrier. The emitter is a 20 nm lightly doped ($2 \times 10^{16} \text{ cm}^{-3}$) InAs layer followed by a heavily doped ($2 \times 10^{18} \text{ cm}^{-3}$) contact. The collector consists of a 75 nm nominally intrinsic region doped for the simulation at $1 \times 10^{15} \text{ cm}^{-3}$ followed by a heavily doped ($2 \times 10^{18} \text{ cm}^{-3}$) contact. A calculated band diagram of the device is shown in Fig. 1. Figs. 2 and 3 show overlaid

NEMO and SPICE simulations of the current-voltage (I-V) and capacitance-voltage (C-V) responses of the RTD. We will, in turn, describe each of these simulations starting with the NEMO simulation.

II. QUANTUM SIMULATIONS

The NEMO simulations use a nearest neighbor 2-band model of the InAs and AlSb materials. The atomic positions are used with one s-symmetry state placed on the cation and one p-symmetry state placed on the anion. This gives a Hamiltonian with alternating positive and negative off-diagonal coupling down the chain resulting in the coupled 2-band model. It is necessary to use such a model since the electron is tunneling through the AlSb closer to the valence band than the conduction band. Integration over the transverse momenta is performed numerically. The coherent transport model is used, and the electron charge is calculated self-consistently by iterating a Green function solution of Schrödinger's equation with Poisson's equation [12], [13]. Deep in the leads, the Fermi level is obtained based on the density of states calculated from the 2-band model. For our test device, the computed full width at half maximum of the transmission at peak current for zero transverse momentum is 7 meV corresponding to a dwell time in the well of 94 fs.

NEMO computes the capacitance by numerically evaluating

$$C = \delta Q / \delta V \quad (1)$$

with a δV of 10 mV. δQ is computed by stepping through the device, one monolayer at a time, keeping separate running sums of the positive and negative differential charge. The total negative differential charge per unit area is calculated as

$$\delta Q^- = a \sum_j (\delta q_j < 0) \quad (2)$$

where a is the monolayer length and δq_j is the differential charge per unit volume on monolayer j . The positive differential charge, δQ^+ , is also computed. As a check, two values of the capacitance are printed out, dQ^+/dV and $|dQ^-/dV|$ which should agree. In general, for capacitance calculations, the convergence tolerance on the electrostatic potential must be set to 1 μ V or less at each monolayer to avoid noise in the numerical derivative. A plot of the differential charge throughout the device at $V=0.8V$ (immediately

preceding the current peak) and $V=1.0V$ (the center of the NDR region) is shown in Fig. 4. Before the peak current, the well acts electrostatically as a continuation of the accumulation layer in the emitter. The increasing negative charge in the emitter and well is imaged by the increasing positive charge in the collector. In the NDR region, the well discharges resulting in a positive differential charge in the well. This positive differential charge in the well is imaged by an increased negative differential charge in the emitter. The magnitude of this differential charge is related to the differential current and thus, the negative conductance.

The NEMO results are used to provide a standard of comparison to verify the compact model. NEMO has been shown to give qualitatively correct results for RTD structures [14], [15]. The same shape and position of the quantum capacitance with respect to the NDR region has been found both theoretically from a self-consistent a.c. Schrödinger / Poisson solution [7] and experimentally [4], [6], [8] by others. Our point is to show that our compact model can reproduce a qualitatively correct C-V curve. The quantitative peak and valley positions are easily adjusted using the input parameters of [2].

III. QUANTUM CAPACITANCE MODEL

Using the NEMO simulations as guidance, we derive a simple compact model for the quantum capacitance, implement it into TSPICE [16], and observe its effects on an oscillator circuit. For the positive differential regions of the RTD I-V, since the quantum well acts electrostatically as an extension of the emitter accumulation, we continue to use the standard model for the depletion capacitance. In the NDR region of the I-V, we add to the depletion capacitance our model for the quantum capacitance. To derive the model, we start with the definition implemented by NEMO, Eq. (1). The quantum capacitance results from the change of charge in the well. Therefore, we calculate the quantum capacitance as

$$C_Q = dQ_W/dV \quad (3)$$

where C_Q is the quantum capacitance per unit area, Q_W is the two dimensional sheet charge in the well, and V is the applied voltage. The RTD current density can be written

as

$$J = -Q_W/\tau_C \quad (4)$$

where τ_C is the escape rate through the collector barrier. Then

$$C_Q = \frac{dQ_W}{dJ} \frac{dJ}{dV} = -\tau_C g = |g| \tau_C \quad (5)$$

where $g = dJ/dV$ is the differential conductance which is less than 0 in the NDR region. This is the form of the quantum capacitance that we use in our SPICE model. For our device, and for many experimental devices, this expression is, for practical purposes, equivalent to the expression found in [9].

The effect of the quantum capacitance on the resistive cutoff frequency is obtained from the analysis of the circuit shown in Fig 5. The resistive cutoff frequency, the maximum frequency of oscillation, which is the frequency at which the real part of the impedance is equal to 0 is given by

$$f = \frac{1}{2\pi |r| (C_D + C_Q)} \sqrt{\frac{|r|}{R_s} - 1} \quad (6)$$

where $r = 1/g$ is the negative differential resistance and C_D is the depletion capacitance. Multiplying through the factor of $|r|$ in the denominator results in

$$f = \frac{1}{2\pi (|r| C_D + \tau_C)} \sqrt{\frac{|r|}{R_s} - 1} \quad (7)$$

This shows how the quantum capacitance reduces the maximum frequency of oscillation. The escape rate through the collector is simply added to the $|r|C_D$ time constant of the negative differential resistance and depletion capacitance.

IV. SPICE SIMULATIONS

What is actually implemented into our SPICE model is given by Eq. (8)

$$C_Q = \begin{cases} |g| \hbar/\Gamma_C & (g < 0) \\ 0 & (g \geq 0) \end{cases} \quad (8)$$

where we have introduced one new parameter, Γ_C , into the list given in Table II of reference [2]. Physically, $\Gamma_C = \hbar/\tau_C$ is the full width at half maximum energy broadening of the state in the well resulting from leakage out of the collector barrier. In this model, Γ_C is

a constant. The NEMO simulations indicate that Γ_C is nearly independent of bias over the NDR region. It changes from 5.72 meV to 6.04 meV, or approximately 5.5%. For our structure, it should be nearly identical to the existing parameter, Γ , the full-width at half maximum of the resonance. The conductance, g , is calculated analytically from the physics based current expression in [2]. Given the compact model, we then choose the parameters in Table I to give the best fit to the NEMO simulations shown in Figs. 1-2. This fitting was performed by hand.

The test circuit that we model is shown in Fig. 6. The cross sectional area of the RTD is $1 \mu\text{m}^2$ which results in a minimum magnitude of the NDR of 140Ω . SPICE simulations were performed with and without the quantum capacitance model for the RTD. The time step used was 50 fs. Figs. 7 and 8 show the results calculated without the quantum capacitance model. SPICE simulations with the quantum capacitance model of Eq. (8) are shown in Figs. 9 and 10. The nonlinear capacitance gives rise to distortion resulting in energy spread out of the fundamental harmonic.

The distortion is the result of the nonlinearity in the capacitance, not the discontinuity in the derivative or the overall magnitude. As the capacitance of the tank becomes much larger than the capacitance of the RTD in Fig. 6, the distortion disappears since the RTD capacitance is negligible compared to the capacitance in the rest of the circuit. To check that the discontinuity in the derivative of the capacitance model was not the cause of the distortion, we have also run SPICE simulations with the quantum capacitance model of

$$C_Q = -g\hbar/\Gamma_C \quad (9)$$

for all voltages. It undershoots somewhat between 0.3 and 0.8 V, but the derivative is continuous. The same distortion in the output voltage appears. The distortion results from the nonlinearity when one is trying to achieve the highest frequency performance such that the RTD capacitance is comparable to the rest of the capacitance in the circuit.

Table I, similar to Table II of [2], lists the parameters that we used in our RTD model for the SPICE simulation. A few parameters are appended to calculate the depletion capacitance change due to the expansion of the depletion region from the lightly-doped layer to the heavily-doped contact. The following formulas are used to model the depletion

capacitance

$$C_D = \frac{AC_{j0}}{\sqrt{1 + \frac{|V|}{V_\phi}}} \quad (10)$$

We introduce into Table 1 the parameter V_C which is the voltage at which the depletion region moves from the lightly doped collector spacer to the heavily doped collector contact. For $V < V_C$, $C_{j0} = C_0$ and $V_\phi = V_{\phi 0}$ where C_0 is the depletion capacitance at zero voltage and $V_{\phi 0}$ is the initial capacitance voltage scale factor. For $V > V_C$, $C_{j0} = C_0/\alpha_C$ and $V_\phi = \beta_{V\phi}V_{\phi 0}$. where α_C and $\beta_{V\phi}$ are scale factors to account for the different doping densities between the lightly doped spacer and heavily doped contact. Since the capacitance is continuous at V_C , in our implementation the user enters only V_C and $\beta_{V\phi}$, and α_C is automatically computed.

In summary, we have presented a simple derivation of a physics-based quantum capacitance model to enhance the physics based RTD SPICE model described in references [1,2]. We have shown how the quantum capacitance reduces the resistive cutoff frequency. We have implemented the model in TSPICE and demonstrated its distorting effect on an oscillator circuit. The effect of the nonlinearity in the RTD capacitance becomes important for the highest frequency applications when the RTD capacitance is comparable to the capacitance in the rest of the circuit.

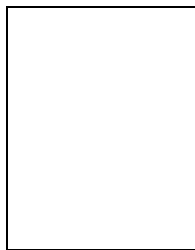
ACKNOWLEDGMENTS

We thank G. Klimeck at NASA JPL for enhancing this version of NEMO for operation on the Linux OS. We thank W. Porod for informing us about the TSPICE software. This work was supported in part by Raytheon and the NSF.

REFERENCES

- [1] J.N. Schulman, H.J. De Los Santos, and D.H. Chow, "Physics-based rtd current-voltage equation," *Electron Device Letters*, vol. 17, no. 5, pp. 220 – 222, 1996.
- [2] T. P. E. Broekaert, B. Brar, J. P. A. van der Wagt, A. C. Seabaugh, F. J. Morris, T. S. Moise, E. A. Beam III, and G. A. Frazier, "A monolithic 4-bit 2gsps resonant tunneling analog-to-digital converter," *IEEE J. Solid State Circuits*, vol. 33, no. 9, pp. 1342 – 1349, 1998.
- [3] R. E. Miles, G. Millington, R. D. Pollard, D. P. Steenson, J. M. Chamberlain, and M. Henni, "Accurate equivalent circuit model of resonant tunnelling diodes," *Electronics Lett.*, vol. 27, no. 5, pp. 427 – 428, 1991.
- [4] J. Genoe, C. Van Hoof, W. Van Roy, J. H. Smet, K. Fobelets, R. P. Mertens, and G. Borghs, "Capacitances in double-barrier tunneling structures," *IEEE Trans. Elect. Dev.*, vol. 38, no. 9, pp. 2006 – 2012, 1991.

- [5] T. Wei, S. Stapleton, and O. Berolo, "Scattering parameter measurements of resonant tunneling diodes up to 40 ghz," *IEEE Trans. Elect. Dev.*, vol. 42, no. 7, pp. 1378 – 1380, 1995.
- [6] T. Wei, S. Stapleton, and O. Berolo, "Equivalent circuit and capacitance of double barrier resonant tunneling diode," *J. Appl. Phys.*, vol. 73, no. 2, pp. 829 – 834, 1993.
- [7] W-R. Liou and P. Roblin, "High-frequency simulation of resonant tunneling diodes," *IEEE Trans. Elect. Dev.*, vol. 41, no. 7, pp. 1098–1111, 1994.
- [8] N. Shimizu, T. Waho, and T. Ishibashi, "Capacitance anomaly in the negative differential resistance region of resonant tunneling diodes," *Jpn. J. Appl. Phys.*, vol. 36, no. 3B, pp. L330 – L333, 1997.
- [9] M. N. Feiginov, "Effect of the coulomb interaction on the response time and impedance of the resonant-tunneling diodes," *Appl. Phys. Lett.*, vol. 76, no. 20, pp. 2904 – 2906, 2000.
- [10] D. K. Blanks, G. Klimeck, R. Lake, D. Jovanovic, R. C. Bowen, C. Fernando, W. R. Frensley, and M. Leng, "Nemo: general release of a new comprehensive quantum device simulator," in *Compound Semiconductors 1997. Proceedings of the IEEE Twenty-Fourth International Symposium on Compound Semiconductors*, New York, 1998, pp. 639–642, IEEE.
- [11] E. R. Brown, J. R. Söderstrom, C. D. Parker, L. J. Mahoney, K. M. Molvar, and T. C. McGill, "Oscillations up to 712 ghz in inas/albs resonant-tunneling diodes," *Appl. Phys. Lett.*, vol. 58, no. 20, pp. 2291–2293, 1991.
- [12] R. Lake, G. Klimeck, R. C. Bowen, and D. Jovanovic, "Single and multi-band modeling of quantum electron transport through layered semiconductor devices," *J. Appl. Phys.*, vol. 81, no. 12, pp. 7845–7869, 1997.
- [13] R. Lake, G. Klimeck, R. Bowen, D. Jovanovic, and D. Blanks, "Quantum transport with band-structure and schottky contacts," *Phys. Stat. Sol. (b)*, vol. 204, no. 1, pp. 354–357, 1997.
- [14] R. Lake, G. Klimeck, R. C. Bowen, C. L. Fernando, D. Jovanovic, D. Blanks, T. S. Moise, Y. C. Kao, M. Leng, and W. R. Frensley, *1996 55th Annual Device Research Conference Digest*, p. 174, IEEE, NY, 1996.
- [15] G. Klimeck, R. C. Bowen, T. Boykin, R. Lake, D. Blanks, T. S. Moise, Y. C. Kao, and W. R. Frensley, *1997 55th Annual Device Research Conference Digest*, p. 92, IEEE, NY, 1997.
- [16] "T-spice pro," <http://www.tanner.com/eda/>.



Roger Lake received his Ph.D. in electrical engineering from Purdue University in 1992 and joined the Nanoelectronics Branch of Central Research Labs, Texas Instruments in Dallas in 1993 to develop the theory for the Nanotechnology Engineering Program which became known as NEMO. In 1997, the Nanoelectronics Branch was acquired by Raytheon where Lake worked on a number of different materials and devices: Si/SiGe tunnel diodes, InGaAs/InAlAs HEMTs for both high speed ADCs and low power memory, InAs/AlSb and InGaAs/InAs/AlAs RTDs for for ADC, TSRAM, and THz applications. Currently, Lake is in the Electrical Engineering Department of the University of California, Riverside working on full-band, 3D modeling of Si/SiGe quantum confined structures, high frequency response of RTDs, molecular electronics, and quantum computing.



Junjie Yang received the M.S. degree in electrical engineering from the Chinese Academy of Sciences, Shanghai, China, in 1996, and the B.S. degree in Physics from East China Normal University, Shanghai, China, in 1993. From 1996 to 2000, he worked in Lucent Technologies Microelectronics Group in China as an IC design engineer on digital and mixed-signal CMOS/BiCMOS projects: SDH/SONET ADM, ADSL transceiver, V.90 Modem/CS4 and switches. He is currently pursuing the Ph.D. degree in electrical engineering at the University of California, Riverside and working as a Researcher Assistant/Teaching Assistant on

high-frequency device Spice modeling and corresponding circuit design and analysis.

Figure Captions

Fig. 1. Calculated band diagram of the InAs / AlSb RTD.

Fig. 2. NEMO and SPICE simulations of the $1 \mu\text{m}^2$ InAs / AlSb RTD I-V response.

Fig. 3. NEMO and SPICE simulations of the $1 \mu\text{m}^2$ InAs / AlSb RTD C-V response.

Fig. 4. Normalized differential charge ($[\rho(V + 10\text{mV}) - \rho(V)] / |e|$) throughout the device at $V = 0.8\text{V}$ (immediately preceding the current peak) and at $V = 1.0\text{V}$ (the center of the NDR region).

Fig. 5. Equivalent small signal model of the RTD with series resistance, R_s , for calculating the resistive cutoff frequency.

Fig. 6. Oscillator circuit. The input voltage is stepped from 0 - 1.1V in 100 ps.

Fig. 7. SPICE simulation of V_{out} versus time starting at $t = 3\text{ns}$ without the quantum capacitance model.

Fig. 8. SPICE simulation of the Fourier spectrum of V_{out} without the quantum capacitance model.

Fig. 9. SPICE simulation of V_{out} versus time starting at $t = 3\text{ns}$ with the quantum capacitance model.

Fig. 10. SPICE simulation of the Fourier spectrum of V_{out} with the quantum capacitance model.

FIGURES

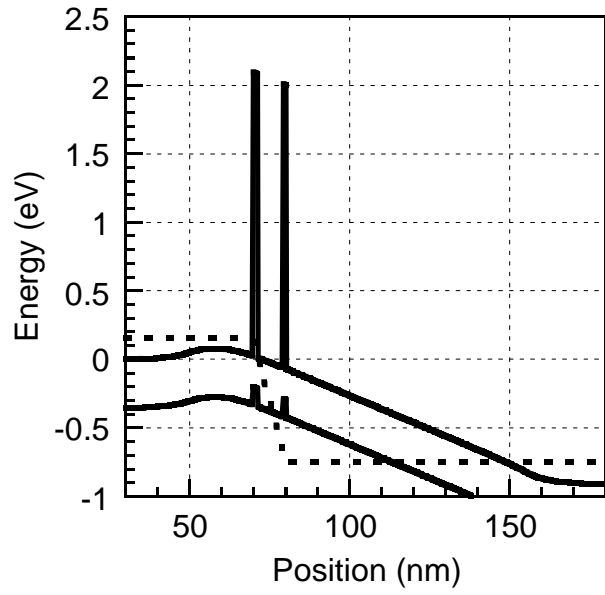


Fig. 1.

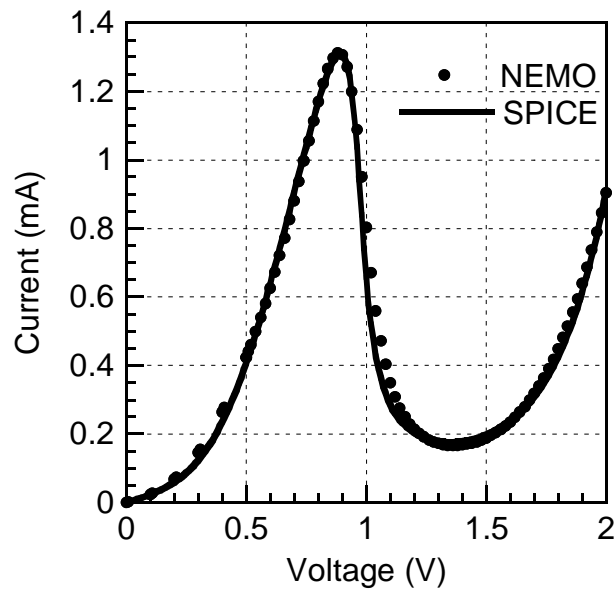


Fig. 2.

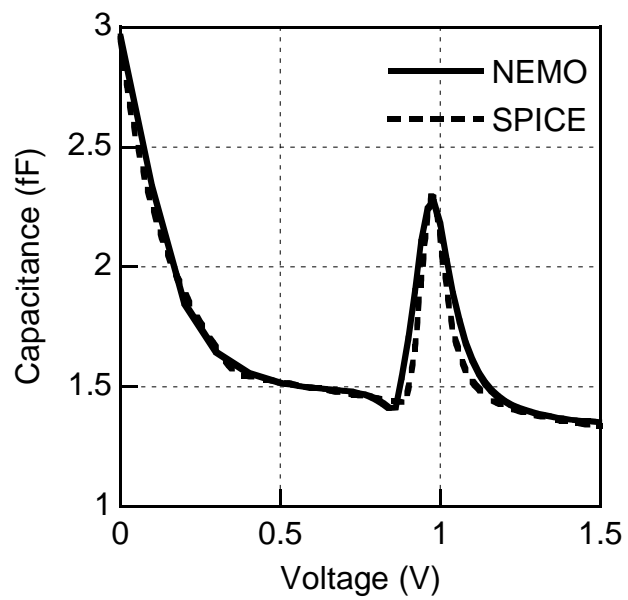


Fig. 3.

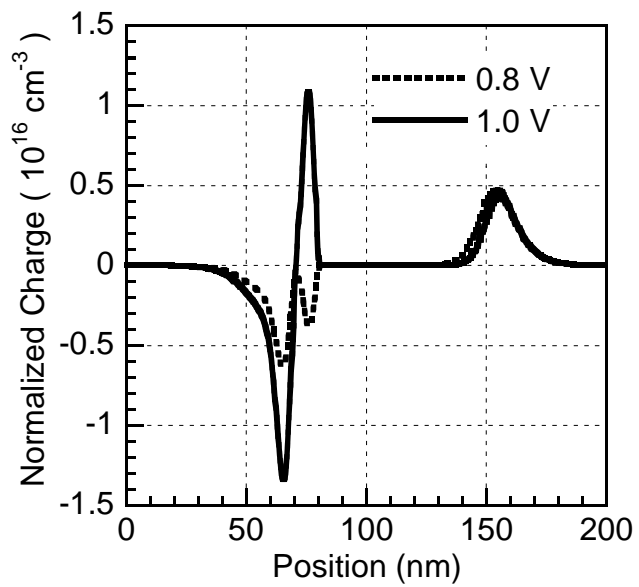


Fig. 4.

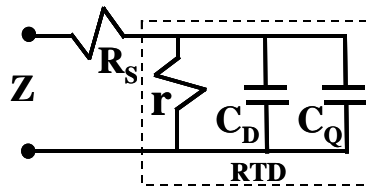


Fig. 5.

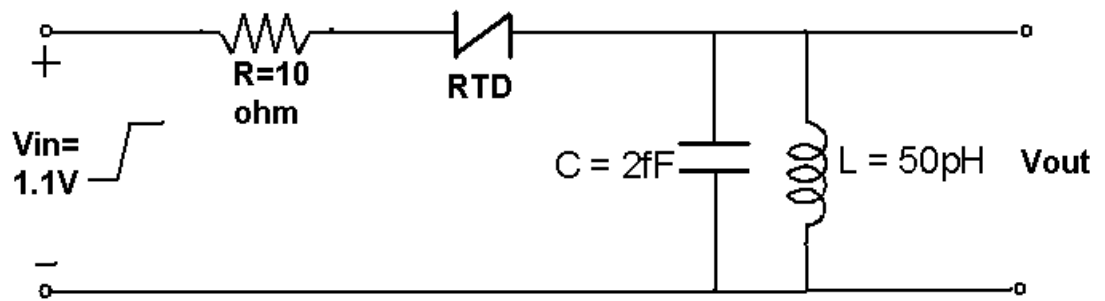


Fig. 6.

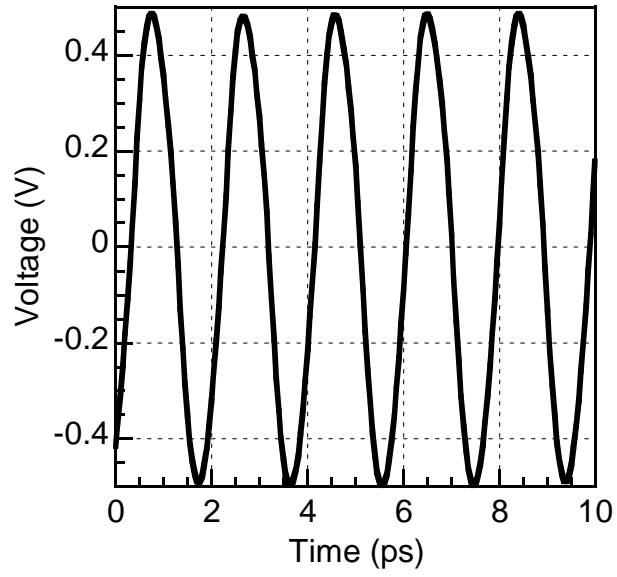


Fig. 7.

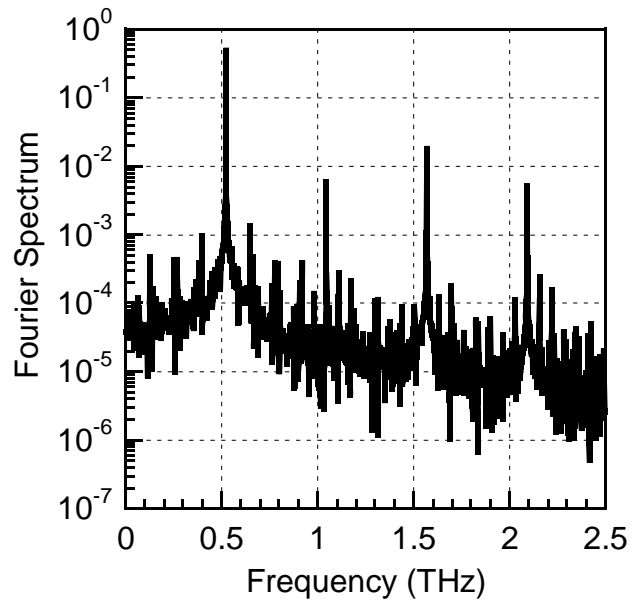


Fig. 8.



Fig. 9.

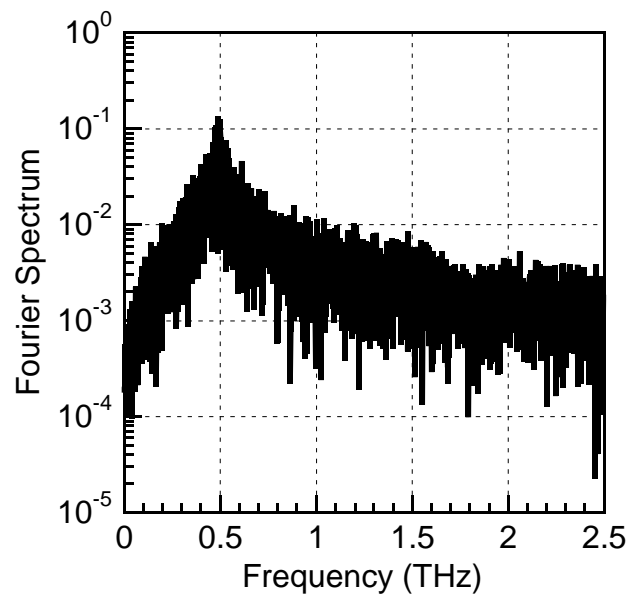


Fig. 10.

Parameter	Description	Value
A	Device Area	$1.0 \mu\text{m}^2$
J_P	Peak Current density	$1.4 \text{ mA}/\mu\text{m}^2$
V_N	Voltage of maximum NDR	0.97 V
V_T	Resonance turn-on Voltage	0.45 V
Γ	Full-width at half maximum of the resonance	50.0 meV
n	Resonance subthreshold ideality or “lever” factor	5.0
J_V	Thermionic leakage current at V_V	$0.05 \text{ mA}/\mu\text{m}^2$
n_V	Thermionic leakage current ideality	8.5
V_v	Valley Voltage	1.38V
kT	Thermal Voltage	26 meV
C_0	Junction Capacitance at zero voltage	$2.95 \text{ fF}/\mu\text{m}^2$
$V_{\Phi 0}$	Initial voltage level	0.14 V
V_C	Switching point for sudden depletion density change	0.36 V
α_C	Junction Capacitance Adjusting factor due to highly doped area	1.78
$\beta_{V\Phi}$	V_{Φ} Adjusting factor due to highly doped area	19
Γ_C	full width at half maximum energy broadening of the state in the well resulting from leakage out of the collector barrier	7.6meV

Table 1. RTD SPICE Model parameters used in the simulation.